

Red-shifted tetra-*ortho*-halo-azobenzenes for photo-regulated transmembrane anion transport

Aidan Kerckhoffs, Zonghua Bo, Samuel Penty, Fernanda Duarte*, and Matthew J. Langton*^a

Received 00th January 20xx,
Accepted 00th January 20xx

DOI: 10.1039/x0xx00000x

Photo-responsive synthetic ion transporters are of interest as tools for studying transmembrane transport processes and have potential applications as targeted therapeutics, due to the possibility of spatiotemporal control and wavelength-dependent function. Here we report the synthesis of novel symmetric and non-symmetric red-shifted tetra-*ortho*-chloro- and tetra-*ortho*-fluoro azobenzenes, bearing pendant amine functionality. Functionalisation of the photo-switchable scaffolds with squaramide hydrogen bond donors enabled the preparation of a family of anion receptors, which act as photo-regulated transmembrane chloride transporters in response to green or red light. The subtle effects of chlorine/fluorine substitution, *meta/para* positioning of the anion receptors, and the use of more flexible linkers are explored. NMR titration experiments on the structurally diverse photo-switchable receptors reveal cooperative binding of chloride in the Z, but not E isomer, by the two squaramide binding sites. These results are supported by molecular dynamics simulations in explicit solvent and model membranes. We show that this intramolecular anion recognition leads to effective switching of transport activity in lipid bilayer membranes, in which optimal Z isomer activity is achieved using a combination of fluorine substitution and *para*-methylene spacer units.

Introduction

Azobenzenes are versatile and robust molecular photo-switches which have attracted significant interest for a wide range of applications, ranging from molecular switches and machines,¹ photo-responsive catalysts,² energy storage,^{3,4} and to control specific biological targets such as to facilitate targeted drug action.^{5,6} Azobenzene itself is switched from the thermally stable E isomer to the Z isomer using UV light; however, for applications in biology, photo-isomerisation should ideally occur in the red or near IR region to optimise tissue penetration and minimise collateral cell damage.^{7,8} Recently, significant research effort has been directed to developing such derivatives, and a number of groups have shown that heteroatom *ortho*-substitution of azobenzenes leads to significant red shifting of the $n-\pi^*$ band of the E isomer, separating it from the Z $n-\pi^*$ transition.^{9–12} This enables visible light-mediated photo-switching by direct excitation of the red-shifted $n-\pi^*$ transition, allowing for Z-rich photo-stationary states to be achieved, and in many cases increasing the thermal half-lives of the Z isomer. For example, tetra-*ortho*-chloro azobenzene¹³ undergoes isomerisation to the Z isomer at a wavelength maxima of ~450 nm, while the tail of the absorption spectra extends sufficiently far into the red region to enable switching at 625 nm (red light). Despite their numerous beneficial properties, synthetic strategies towards such systems remain relatively limited,^{14–16} and in many cases low yielding, because of challenges in forming sterically congested N=N double bonds surrounded by chlorine substituents. This is

particularly true for common azo-coupling¹³ or oxidative aniline dimerisation strategies.^{14,17} Furthermore, whilst there has been much work exploring the effect of heteroatom substitution on photo-switch properties,¹⁸ considerably less effort has been devoted to developing derivatives with one or more functional handles for further derivatisation. Non-symmetric red-shifted azobenzene derivatives with orthogonal functional handles – necessary for linking different chemical motifs with a photo-switchable linker – are particularly rare.^{19–21}

Supramolecular anionophores that act as mobile anion carriers have been the target of significant recent research effort. This has been driven by applications in therapeutics, such as for cancer treatment and diseases arising from mis-regulated ion channels (channelopathies), including cystic fibrosis, or as tools for studying ion transport processes.^{22–25} These carriers facilitate ion transport down a concentration gradient by lowering the kinetic barrier to transmembrane transport. This is achieved by binding of the ion within a lipophilic receptor through typically hydrogen bonding (HB),²⁶ and recently sigma-hole,^{27–29} interactions. The carrier-ion complex diffuses across the bilayer to release the ion on the opposite side of the membrane.

Stimuli-responsive anion carriers have attracted particular recent interest as a means to spatio-temporally control their function.³⁰ A handful of examples of such systems responsive to pH,³¹ membrane potential,³² enzymes,³³ reduction,³⁴ and UV light^{35,36} have been reported. Photo-switchable anion receptors, in which there is enhanced binding of the anion to one of the two photo-isomers,^{37–44} offer a route towards switchable transporters in which the system can be reversibly switched between inactive (OFF) and active (ON) states. To this end, we recently exploited red-shifted azobenzenes functionalised with HB donor squaramide motifs to develop the first photo-responsive synthetic anion transporter that is reversible switched ON and OFF by photo-isomerisation using red and blue light, respectively.⁴⁵

Here, we report the synthesis of symmetric and non-symmetric red-shifted amino-functionalised azobenzenes that

^a Department of Chemistry, University of Oxford.

Chemistry Research Laboratory, 12 Mansfield Road, Oxford, OX1 3TA

Email: matthew.langton@chem.ox.ac.uk. Computational correspondence to

Fernanda.duarte@chem.ox.ac.uk.

Electronic Supplementary Information (ESI) available: [details of any supplementary information available should be included here]. See DOI: 10.1039/x0xx00000x

are photo-switched with red or green light, and apply these scaffolds to develop novel visible-light activated transporters with enhanced activity and function. We explore the role of cooperative anion binding in the photo-regulated transport process using a range of transporters of different geometries and control compounds through detailed binding studies, transport experiments and computational studies.

Approach

We have previously reported photo-switchable transmembrane ion transporter **1a** (Fig. 1). This transporter, which acts as a switchable mobile anion carrier, exhibits an 8-fold enhancement in activity for the *Z* isomer over the *E* isomer in ion transport assays. This enabled unprecedented *in-situ* OFF-ON reversible switching of transport activity in lipid bilayer membranes to be achieved by irradiation with red (ON) and blue (OFF) wavelengths of light. However, background activity of the *E* isomer at higher loadings in the membrane proved significant, and attempts to enhance transport activity by addition of electron withdrawing groups to the squaramide H-bond donors diminished the *Z/E* discrimination in transport rates. In this work, we sought to explore and understand the role of the azobenzene structure in cooperative binding of the anions, with the aim of enhancing both overall activity of the system and the differentiation in activity between the *E* isomer (OFF) and *Z* isomer (ON) in order to achieve efficient photo-switchable transport. In transporter **1a**, the aryl-squaramide HB donor motifs are appended to the photo-switchable azobenzene core via methylene spacers, because direct conjugation of anion binding motifs to the azobenzene is known to significantly decrease the lifetime of the *Z* isomer.³⁹ To explore the role of cooperative anion binding on transport efficiency, we varied the linker length and position on the azobenzene core (compounds **2** and **3**) and the nature of the azobenzene substituents (**1b**), and employed compound **4**, in which the second anion-binding site is removed, as control.

Synthesis

Synthesis of tetra-*ortho*-fluoro derivative **1b**

Squaramide derivatives are typically accessed via condensation of a primary amine with a pre-formed mono-squaramide, itself prepared from a dialkoxysquarate derivative.⁴⁶ Transporter **1a**⁴⁷ was prepared from the corresponding bis-amino-azobenzene, which was accessed via a *N*-chlorosuccinimide (NCS)-mediated oxidative coupling⁴⁸ of Boc-protected-(aminomethyl)-substituted-2,6-dihaloaniline. This strategy also proved to be applicable to the synthesis of tetra-*ortho*-fluoro azobenzene anionophore **1b** (Scheme 1). Microwave-assisted cyanation of **5** afforded nitrile **6**. Reduction of **6** with borane gave rise to amine **7**, which proved to be unstable and thus was immediately Boc-protected to provide compound **8**. NCS-mediated oxidative coupling⁴⁸ of **8** generated tetra-*ortho*-fluoroazobenzene **9**, which was subsequently deprotected to **10** and coupled to mono-squaramide **11** to afford the desired compound **1b**. Full

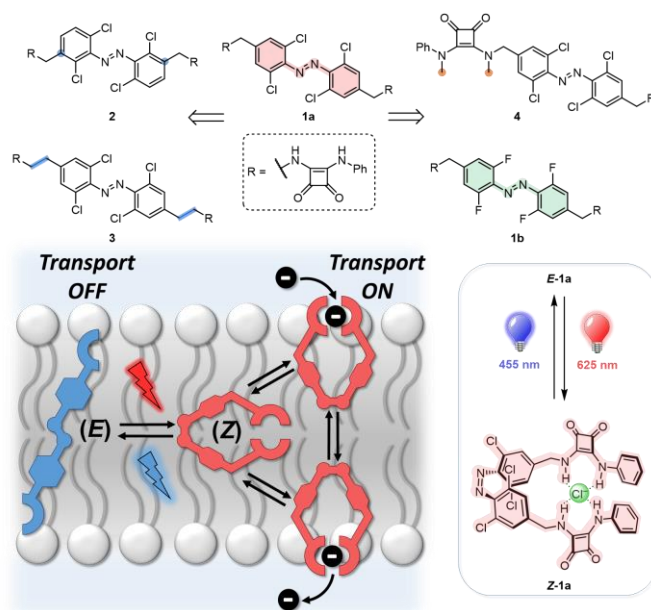
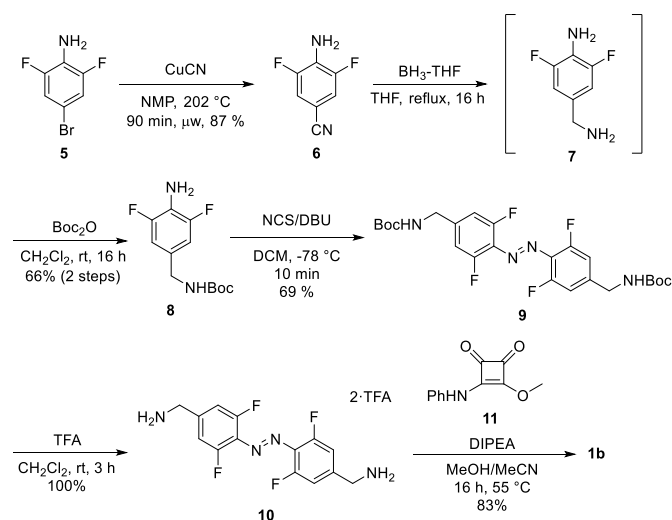


Figure 1. Red-shifted azobenzenes as photo-switchable ion transporters. **Top:** Transporters studied in this work. **Bottom:** Schematic representation of the photo-switching of a supramolecular ion carrier

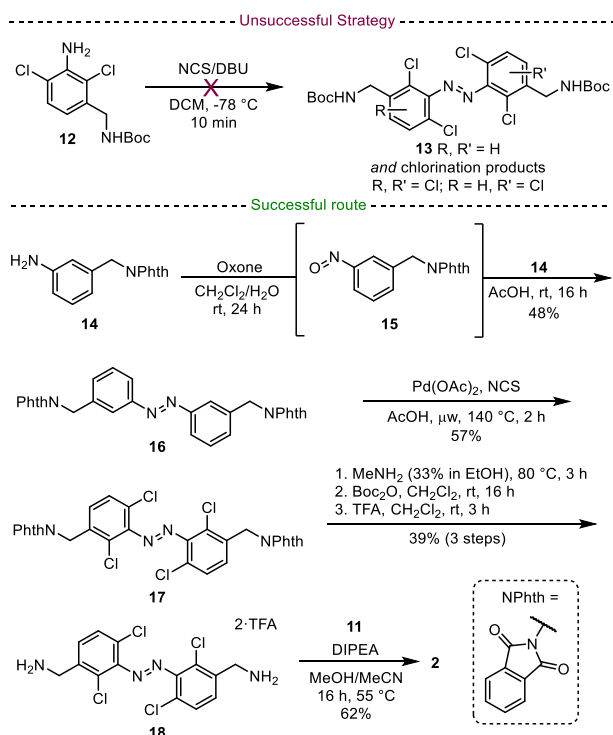


Scheme 1. Synthesis of tetra-*ortho*-fluoro azobenzene anionophore **1b**

synthetic details and characterisation are available in the Supplementary Information.

Synthesis of *meta*-substituted azobenzene **2**

To prepare *meta*-substituted amino-methyl azobenzene derivative **2**, we initially sought to employ the same NCS-mediated oxidative coupling strategy used to prepare compound **9** on compound **12**. This strategy led to formation of the desired tetra-*ortho*-chloro azobenzene **13** but also undesired over-chlorinated products, which could not be readily separated via column chromatography (Scheme 2, top). This is presumably due to electrophilic aromatic chlorination of the electron rich aniline or partially oxidised hydrazine intermediate prior to azobenzene formation, despite reports of simple *meta*-substituted anilines successfully forming under these conditions.⁴⁸ Alternative oxidative coupling conditions

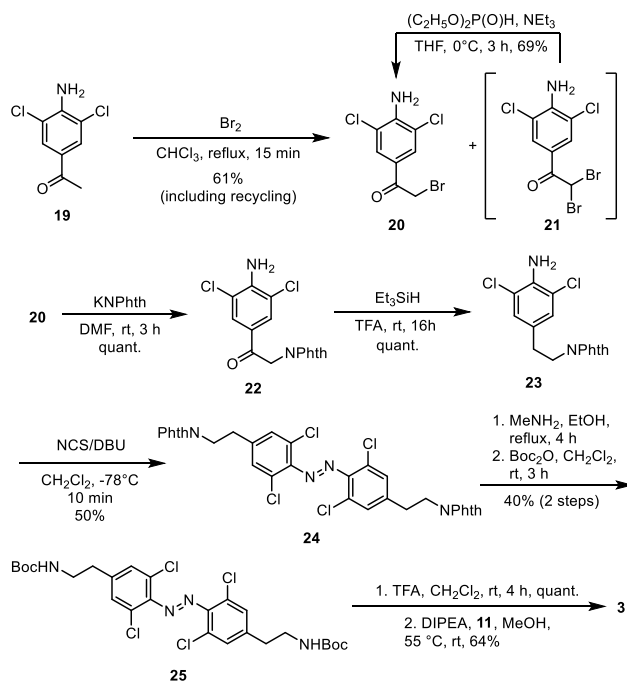


Scheme 2. Synthesis of meta-substituted azobenzene 2

using sodium perborate and catalytic sodium molybdate were also unsuccessful. Pleasingly, a late-stage functionalisation strategy developed by Trauner and co-workers,¹⁵ in which *ortho*-chloro substituents are installed after azobenzene synthesis, proved to be a fruitful approach (Scheme 2, bottom). A Mills reaction of phthalimide-protected amino-methyl aniline **14** and nitroso-derivative **15** provided azobenzene **16**. Microwave-assisted palladium catalysed C-H chlorination on this sterically hindered substrate generated compound **17**. The phthalimide groups were readily removed with methylamine but purification of the corresponding bis-amine was unsuccessful, and so the mixture was therefore *N*-Boc-protected, purified, and subsequently deprotected with TFA to furnish **18**. Finally, coupling to mono-squaramide **11** afforded the desired *meta*-substituted analogue **2**.

Synthesis of ethyl-linked azobenzene 3

Azobenzene **3**, in which the squaramide motifs are appended to the azobenzene core via ethyl linkers, was prepared via an NCS-mediated oxidative coupling strategy (Scheme 3). Bromination of commercially available ketone **19** provided **20**, in addition to the doubly-brominated **21**. It was possible to convert this undesired by-product to the desired **20** under Atherton–Todd conditions. Bromo-ketone **20** was treated with potassium phthalimide to install the protected amino unit **22**, followed by reduction of the aromatic ketone *via* an acidic hydrosilane reduction to afford **23**. Oxidative coupling of **23** generated the



Scheme 3. Synthesis of ethyl linked ionophore 3

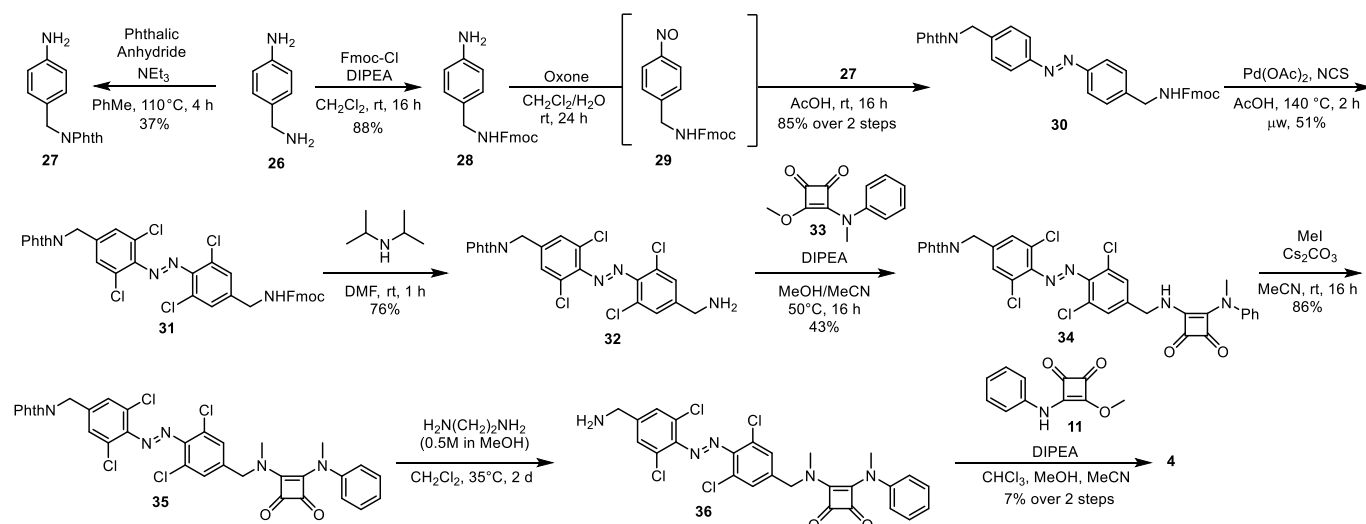
symmetrical *ortho*-chloro azobenzene **24**. Transformation of the phthalimide group to its Boc-protected analogue **25** enabled successful purification, in a similar strategy to that used in the isolation of compound **18**. Deprotection of the Boc protecting groups and condensation with the mono-squaramide **11** provided the final compound **3**.

Synthesis of orthogonally protected non-symmetric azobenzene and control receptor 4

To investigate the role of anion binding cooperativity within the transport process, we prepared a control compound in which the HB donors of one of the squaramide motifs were removed by methylation (compound **4**). This required the development of a novel synthetic route to access non-symmetric tetra-*ortho*-chloroazobenzenes with *para*-aminomethyl substituents protected with suitable orthogonal protecting groups. Due to the inherent difficulties of a late-stage desymmetrisation, it was necessary to build the non-symmetric azobenzene core early in the synthesis.

Fluorenylmethyloxycarbonyl (Fmoc) and phthalimide protected building blocks **27** and **28** were identified as plausible starting points due to their orthogonal deprotection conditions and resistance to the relatively harsh acidic C-H chlorination step. Furthermore, the phthalimide group blocks both reactive positions on the nitrogen atom, enabling a late-stage squaramide methylation.

Protected aminomethyl-aniline derivatives **27** and **28** were coupled using a Mills reaction to generate azobenzene **30**, which was efficiently chlorinated using microwave-assisted C-H chlorination to afford tetra-*ortho*-chloro azobenzene **31**.^[67] Selective Fmoc deprotection using diisopropyl amine afforded



Scheme 4. Synthesis of non-symmetric azobenzene derivatives

32, which was subsequently reacted with methylated monosquaramide **33**, itself generated in 1 step from *N*-methylaniline and dimethyl squarate. Prior to phthalimide deprotection, squaramide *N*-methylation of **34** using methyl iodide gave **35**, which was followed by phthalimide deprotection with ethylene diamine to afford **36**. This bis-amine species proved to be relatively unstable, particularly above 40°C, but immediate reaction with mono-squaramide **11** afforded the desired control compound **4**.

Photo-switching experiments

We first examined photo-switching behaviour of the novel red-shifted azobenzenes. Irradiation of the *E* isomer of *ortho*-fluoro azobenzene **1b** with green light (530 nm) afforded *Z*-rich photo-stationary states (77% *Z*), while irradiation with 405 nm light reversed this process (80% *Z* → *E*). Similarly, as with the known photoswitch **1a**,⁴⁵ irradiation of **2** and **3** with red light (625 nm) afforded similar *Z*-rich PSSs (77% and 72% *Z*, respectively), while switching is reversed using blue light (80-86% *Z* → *E*). The UV vis spectra for *ortho*-fluoro azobenzene **1b** are shown in Figure 2, all other spectra and photo-stationary state compositions are available in the ESI. Red-shifting of the *n*-π* transition is observed, whilst the separation of the *E* *n*-π* from the *Z* *n*-π* transitions enables efficient switching.⁹

Anion Binding Studies

With the ditopic photo-switchable anion receptors **1a**, **1b**, **2** and **3** in hand, we investigated the chloride binding capabilities of the receptors by NMR titration experiments. All four ditopic receptors proved to be insoluble in apolar solvents, but were soluble up to approximately 4mM in DMSO. Therefore, the chloride binding capability of the *E* and *Z* isomers was determined by ¹H NMR titration experiments in d₆-DMSO. Aliquots of tetrabutylammonium chloride were added to a

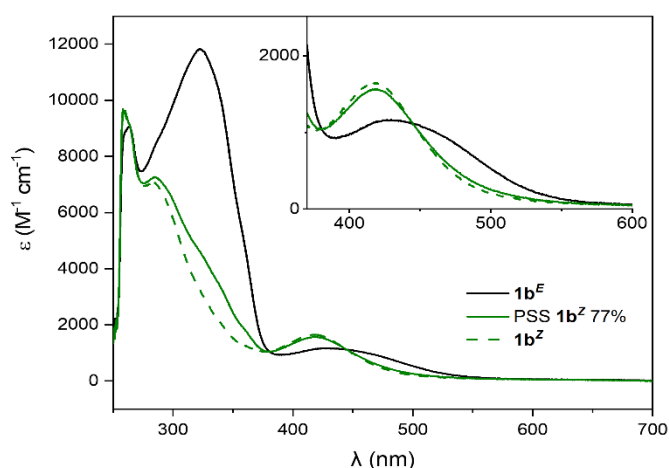


Figure 2. Absorption spectra of **1b** as the *E* and *Z* isomer, and the PSS mixture in DMSO at 25 °C. Inset: *n* → π* bands and composition of the PSS mixtures upon irradiation with red light (530 nm, determined by NMR integration). Pure *Z*-isomer spectrum was calculated from the spectra of pure **1b^E** and the PSS mixture of known composition.

1 mM solution of the receptor and the binding induced chemical shift perturbations monitored. For both isomers, the data fitted satisfactorily to a 1:1 binding isotherm. The chloride binding constants for the *Z* isomer were obtained by conducting the titration with the photo-stationary state mixture formed by irradiating the sample in the NMR tube with 625 nm light (530 nm for **1b**), and the binding competition to the minor population of *E* isomer was accounted for in the analysis (see ESI for data and binding models). Chloride binding in DMSO to the *E* isomer of the squaramide receptors was relatively weak (*K*₁ < 200 M⁻¹ in each case, Table 1), and binding of a second anion was too weak to be determined. Anion binding titrations were also conducted with the reference system **4**, in which one of the two squaramide motifs is methylated and therefore unable to bind chloride (Table 1).

Table 1. Anion binding and photo-switch properties

	Receptor						
	1a	1b	2	3	4	37	38
K_{obs}^E (M ⁻¹) ^a	180±4	158±8	134±2	102±6	166±18	165±7	130±6
K_{obs}^Z (M ⁻¹) ^a	267±3	210±5	183±5	142±2	165±11	-	-
K_{refEM}^b	1.6	1.3	1.1	1.1	-	-	-
PSS ratio (Z:E) ^c	77:23	77:23 ^d	77:23	72:28	77:23	-	-

^a Observed 1 : 1 association constant for chloride binding in d₆-DMSO. Errors at the 95% confidence limit. ^b $K_{\text{ref}} = K_{\text{obs}}$ (**37**) for compounds **1a**, **1b**, and **2**; $K_{\text{ref}} = K_{\text{obs}}$ (**38**) for compound **3**. ^c Photo-stationary state determined by NMR integration following irradiation at 625 nm using a high powered LED. ^d Irradiation at 530 nm.

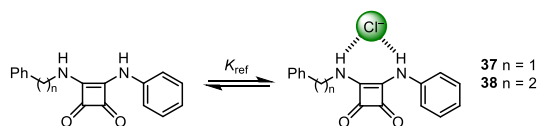


Figure 3. Single binding site squaramide reference compounds **37** and **38**. K_{ref} is the intermolecular association constant for binding of chloride to one squaramide motif.

We also prepared and studied **37** and **38** (Figure 3), which similarly have one available binding site. The observed 1:1 binding constants for the *E* isomers of the ditopic receptors **1a**, **1b**, **2** and **3** are consistent with the single site reference binding constants obtained from these model systems. The enhancement in binding affinity upon photo-switching from *E* to *Z* for the ditopic hosts **1a**, **1b**, **2** and **3**, albeit modest, points to cooperative anion binding in the *Z* isomer by formation of intramolecular hydrogen bonds to the anion from the second squaramide. Blocking the hydrogen bond donors of one of the two squaramide binding sites by methylation (compound **4**) afforded the same binding affinities with both photo-isomers, providing further evidence for intramolecular anion binding by hydrogen bonds from both squaramide motifs in the ditopic systems. This intramolecular interaction may be quantified through the effective molarity, EM (Equation 1), which defines the concentration at which simple intermolecular interactions compete with cooperative intramolecular interactions.⁴⁹

Equation 1. $EM = K_{\text{obs}}^Z / K_{\text{ref}}^2$

The product $K_{\text{ref}}EM$ (Table 1) determines the extent to which the receptor-anion complex with cooperative intramolecular hydrogen bonds from both squaramides is populated, and is broadly similar across all four compounds, albeit with a slight trend of decreasing cooperativity for the *meta* and *para*-ethylene derivatives.[†] This analysis suggests that changes in the azobenzene substitution pattern (from *para*-methylene to *meta*-methylene), or increased spacer length, do not increase the chelate cooperativity in the system.

To further explore the enhanced binding affinity of the *Z* isomers, **1a^Z** was modelled as a representative system in its free form and in complex with chloride. For each system, explicitly solvated (DMSO) molecular dynamics (MD) simulations were propagated over 1 μs (5 × 200 ns).^{50–54} The conformations observed during the simulation were categorised into three

states: an open conformation ($d_{\text{RR}} = 25 \text{ \AA}$), semi-close ($d_{\text{RR}} = 15 \text{ \AA}$), and closed ($d_{\text{RR}} = 6 \text{ \AA}$), where d_{RR} corresponds to the distance between the *para* carbons of the squaramide phenyl rings.

For the free ligand, an open conformation is achieved after only 2 ns, despite the simulation being initiated from a closed conformation, with both squaramide motifs pointing inwards. For the rest of the MD simulation, **1a^Z** remains in an open or semi-close conformation which maximises hydrogen bond (HB) interactions with DMSO (Figure 4, see SI for further details). The **1a^Z•Cl⁻** complex predominantly exists in a closed conformation, enabling a two-site binding mode with 4 HB interactions between the chloride anion and the squaramide NH protons (coordination number, CN = 4). Only in 1 of the 5 simulations, chloride is observed to dissociate, leading to a transient one-site binding (CN = 2) state, followed by complete dissociation of the chloride anion (see SI, Figure S149). Analogous simulations on transporters **2** and **3** afforded similar results, with four HB interactions to the anion in each case (Figure S152–153). Together, these results are consistent with our experimental binding data which reveal stronger binding of the *Z* isomers compared to the *E* isomers and suggest that this is due to the formation of up to 4 HBs in the *Z* isomer.

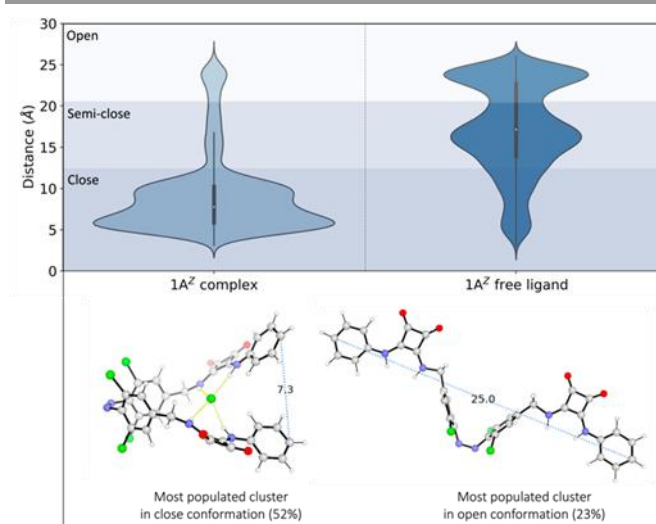


Figure 4. Top: Distance histograms of the end-to-end distance of **1a^Z** as a 1:1 complex with a chloride anion (left) and as a free ligand (right) over 5 replicates of 200 ns simulation in DMSO, resulting in 1 μs of total sampling time per system. Bottom: The structure and percentage population of the most populated clusters of **1a^Z** as a 1:1 complex with a chloride anion and as a free ligand, with their corresponding d_{RR} shown as blue dash lines. Cluster analysis was performed and identifies 60 clusters with a cut-off of 2 Å.

Anion Transport Studies

The binding data suggests that the Z isomers of all four ditopic receptors bind the chloride anion via intramolecular hydrogen bonds to both squaramide binding sites, but that structural variations did not have a significant effect on the effective molarity of the binding interactions. To explore the effect of these variations on the ability of the compounds to act as photo-regulated transmembrane ion transporters, we performed fluorescence anion transport assays in large unilamellar vesicles.

Anion transport assays

The anion transport activities of **1b**, **2**, **3** and **4** were determined using an identical procedure to that for compound **1a** previously reported,⁴⁵ using 1-palmitoyl-2-oleoyl-sn-glycero-3-phosphocholine large unilamellar vesicles (POPC LUVs, lipid concentration 31 μ M), buffered to pH 7.0 in NaCl solution. These LUVs were loaded with 8-hydroxypyrene-1,3,6-trisulfonate (HPTS), a pH sensitive fluorophore which allows for ratiometric determination of the internal pH of the LUVs. A pH gradient was applied across the membrane by addition of a base pulse, followed by addition of the carrier as a DMSO solution (<0.5% v/v). The ability of the carriers to dissipate the pH gradient by transmembrane ion transport was determined by the change in the HPTS emission, I_{rel} ($\lambda_{\text{em}} = 510$ nm), with time following excitation at $\lambda_{\text{ex}} = 405/465$ nm. Lysis of the vesicles using detergent (Triton X-100) at the end of each experiment was used for calibration. For the Z isomers, the experiment was run using the Z-rich PSS mixture.

This assay was used to determine the concentration dependence of the activity of the E and Z isomers of each anion carrier, by adding increasing concentrations of the transporter in DMSO (representative data for **1b** shown in Figure 5, data for all other compounds is available in the Supplementary Information). The fractional activities (y , the relative intensity at 288 s, immediately prior to lysis) were plotted as a function of concentration and the dose-response curves fitted to the Hill equation (Equation 2).

$$y = y_0 + (y_{\text{max}} - y_0) \frac{x^n}{\text{EC}_{50}^n + x^n}$$

Equation 2:

This equation describes the dependence of the anion transport activity (reported by I_{rel}) on the n -th power of the carrier concentration and enables quantitative evaluation of the relative activities of carriers through an effective concentration value (EC_{50}) required to reach 50% activity. EC_{50} values for each compound are given in Table 2, entries 1 – 4, and the corresponding Hill coefficients in entries 5 and 6. Note that the measured $\text{EC}_{50}^{\text{Z,PSS}}$ provides a lower limit of the intrinsic transport ability of the Z isomers of the carriers, with the actual activity up to $\sim 1.25\times$ higher ($\text{EC}_{50} \sim 0.8\times$ smaller) due to the incomplete isomerisation to the Z isomer in the PSS.

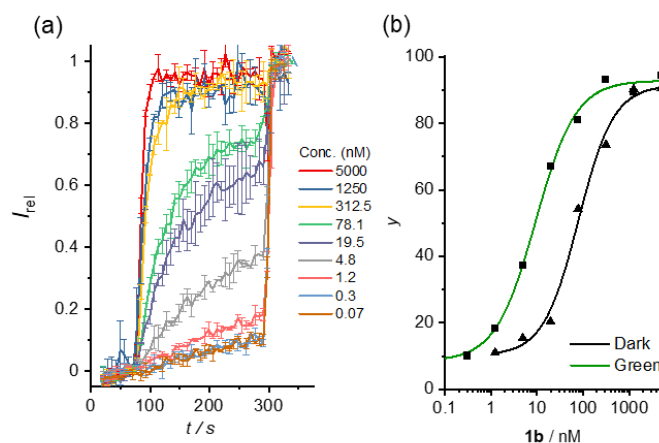


Figure 5. Representative transport data for carrier **1b**. (a) Change in ratiometric emission I_{rel} ($\lambda_{\text{em}} = 510$ nm; $\lambda_{\text{ex1}} = 405$ nm, $\lambda_{\text{ex2}} = 460$ nm) upon addition of **1b^Z** in DMSO to POPC LUVs (31 μ M) containing 1 mM HPTS, 100 mM internal and external NaCl, buffered with 10 mM HEPES at pH 7.0. A pH gradient is generated by addition of a NaOH base pulse (5 mM), followed by the carrier in DMSO. Lysis by Triton X-100 calibrates the assay. (b) Dependence on I_{rel} immediately prior to lysis, y , on concentration of **1b^E** (\blacktriangle) and **1b^Z** (\blacksquare), and fit to the Hill equation (black and green solid lines, respectively).

The enhancement in transport activity on switching from the E to Z isomer for each compound is quantified by the ratio $\text{EC}_{50}^{\text{E}}/\text{EC}_{50}^{\text{Z,PSS}}$ (Table 2, entry 7). Hill coefficients of ~ 1 for all four Z isomer carriers **1a^Z**, **1b^Z**, **2^Z** and **3^Z**, and the control compound **4**, are consistent with results from titration, calculation and transport assays, and point to monomeric transporters at work. Control experiments were also conducted to confirm that the transporters act as mobile anion carriers. Replacing the chloride anion in the buffer with gluconate, which is too hydrophilic to be transported, inhibited transport. This demonstrates that, as with **1a**, all transporters operate via an anion transport mechanism (and not H^+/M^+ cation antiport). Transport activity at 25 $^{\circ}\text{C}$ with each anionophore, as both the E and Z isomers, was negligible in gel phase dipalmitoylphosphatidylcholine (DPPC) lipid vesicles under otherwise identical conditions. Restoration of activity at 45 $^{\circ}\text{C}$, above the gel to fluid phase transition for DPPC lipids of 41 $^{\circ}\text{C}$, provides evidence of a mobile carrier mechanism. Inactivity in a calcein leakage assay of each anionophore rules out non-specific leakage by these systems (See the Supplementary Information).

Structural effects on photo-switchable anion transport

Tetra-ortho-chloro derivative **1a** with para-methylene spacers exhibits an 8-fold enhancement in activity upon photo-switching from the Z to the E isomer ($\text{EC}_{50}^{\text{E}}/\text{EC}_{50}^{\text{Z,PSS}} = 8$, Table 2). Changing from tetra-ortho-chloro (**1a**) to fluoro (**1b**) substitution on the azobenzene core enhanced the overall activity of both isomers by a factor of 2, but did not alter their relative activities ($\text{EC}_{50}^{\text{E}}/\text{EC}_{50}^{\text{Z,PSS}} = 8$ in each case). Calculated $\log P^{\text{SS}}$ values for **1a** and **1b** are 6.8 and 5.2, respectively. This suggests that the reduction in lipophilicity for the fluoro compound is beneficial for transport activity, and indeed a value

Table 2. Transport characteristics of photo-switchable anion carriers **1**, **2**, **3** and **4**.

Entry	Characteristic	Anion transporter				
		1a^d	1b	2	3	4
1	EC ₅₀ ^E (nM) ^a	181 ± 16	79±16	5.2±0.3	11.2±1.1	138±15
2	EC ₅₀ ^E (mol%) ^a	0.58	0.25	0.016	0.036	0.44
3	EC ₅₀ ^{Z,PSS} (nM) ^{a,b}	22 ± 2	9.3±1.0	1.5±0.1	11.7±1.3	123±18
4	EC ₅₀ ^{Z,PSS} (mol%) ^{a,b}	0.071	0.03	0.005	0.038	0.39
5	n ^E ^c	2.6±0.5	1.1± 0.2	1.1±0.1	1.0±0.1	1.2± 0.1
6	n ^Z ^c	1.1±0.1	1.0± 0.1	1.4±0.1	1.2±0.2	1.3± 0.3
7	EC ₅₀ ^E /EC ₅₀ ^Z	8.2±1.0	8.5±2.0	3.3±0.3	1.0±0.1	1.2±0.2

^a Effective concentration to reach 50% of maximal activity in the HPTS assay, reported as both an absolute concentration and mol% relative to lipid. LUVs of POPC (mean diameter 200 nm, lipid concentration 31 μM) loaded with 1 mM HPTS, NaCl (100 mM) and buffered at pH 7.0 with 10 mM HEPES. ^b For the Z isomer, EC₅₀^{Z,PSS} indicates apparent value achieved by addition of the Z-rich PSS mixture. ^c Hill coefficient. ^d Data for previously reported compound **1a** taken from reference ⁴⁵

of ~5 has previously been shown to be an optimum balance of achieving sufficient lipophilicity to embed into the membrane, without suffering from poor membrane delivery or reduced mobility that results from higher transporter lipophilicity.⁵⁶ Deletion of one of the two squaramide chloride binding sites by methylation (compound **4**) removes any enhancement in transport activity for the Z isomer (EC₅₀^E/EC₅₀^{Z,PSS} = 1.2), due to a lack of cooperative binding of the anion by both squaramide motifs, in agreement with results from titration.

Estimation of the effective concentration of the transporters under the assay conditions in the membrane reveals that this is ~40,00-fold higher than in bulk because the transporters are confined only to the small volume occupied by the membrane itself (see ESI for details).⁵⁷ Intra-molecular interactions to chloride by both squaramide motifs are expected to be favoured at a membrane concentration below the effective molarity (~10 mM), assuming this is not significantly affected by the membrane environment. This equates to a total bulk concentration of transporter of <250 nM, which is significantly greater than the EC₅₀ for compounds **1–3**. This analysis suggests that intramolecular chloride binding is likely to be favoured in the membrane. This is in agreement with results of the transport assays, which reveal enhanced transport activity for the Z isomers over E for **1a**, **1b** and **2** which exhibit cooperative chloride binding, but not for compound **4** where this cooperativity is lost.

Changing the substitution pattern of the squaramide receptors on the AB core from *para* (compound **1a**) to *meta* compound **2** increased the transport rate, with the Z isomer exhibiting high overall activity (EC₅₀ = 1.5 nM), but with a reduced ratio between Z and E isomer activity (EC₅₀^E/EC₅₀^{Z,PSS} = 3.3). Extending the alkyl spacer from methylene (**1a**) to ethylene (**3**) also enhanced transport activity, but there was no measurable difference in activity between either isomer in the anion transport assays (EC₅₀^E/EC₅₀^{Z,PSS} = 1). This suggests that, unlike in DMSO solution, the second squaramide anion binding site is not involved in binding to the anion within the bilayer.

It is noteworthy that for **1a**, **1b** and **2**, the enhanced transport efficiency of the Z isomer over E is larger than expected solely from the results of binding titrations (i.e. EC₅₀^E/EC₅₀^{Z,PSS} > K_{ref}EM). Efficient anion carriers require not only strong anion binding affinity, but also must screen the anion charge from the apolar lipid phase, such as by encapsulation within a hydrophobic receptor.⁵⁸ The enhanced encapsulation of the anion by the Z isomer of the transporters, which are also further able to delocalise the anion charge over both squaramide motifs, presumably contributes to the observed enhanced transport efficiency of the Z over the E isomers.

MD simulations of **1a^E** dimerisation

Given the high effective concentration of the transporters when confined in the membrane, and the lower polarity of the membrane compared to DMSO solution in which the titrations were conducted, it is also likely that the E isomers in particular have a propensity to form inactive species in the membrane via inter-molecular hydrogen bonds (dimers or higher-order aggregates). Indeed, squaramide derivatives are well known to form strong, bidentate intermolecular hydrogen bonds, and often have poor solubility in non-polar solvents.^{46,59} Chemical shift perturbations of the squaramide NH protons in NMR dilution experiments in DMSO with **1a^E** were small (<0.05 ppm), suggesting minimal dimerization in this polar media, and unfortunately attempts to characterise intermolecular interactions in less polar solvents were hampered by low solubility. However, it is noteworthy that a modest enhancement in transport activity of methylated **4^E** compared to **1a^E** is observed (138 vs 180 nM). We suggest that this is due to a reduction in the formation of inactive aggregates when one of the two squaramide HB donors is blocked by methylation. This supports our hypothesis that competitive formation of such dimeric or aggregated species are important for suppressing the transport activity of the E isomer.

We explored this idea by conducting MD simulations of **1a^E** dimer in DMSO solution and within a model POPC bilayer.⁶⁰ The

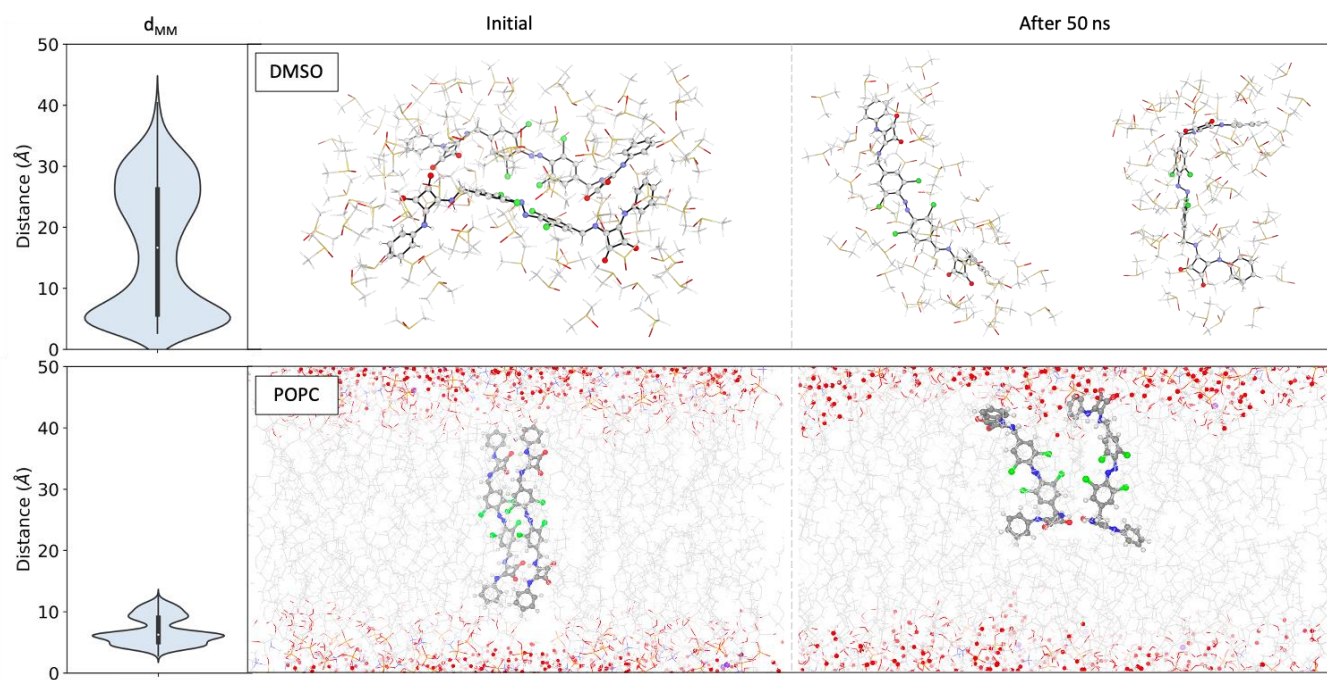


Figure 6. Distance distribution between the center of mass (COM) of the two **1a^F** monomers, d_{MM} , over 5 replicates of 50 ns MD simulations, resulting in 250 ns of total sampling time.; and the corresponding snapshots of the **1a^F** dimer at the start and end of a 50 ns explicitly solvated MD simulation in DMSO (top) and a POPC membrane (bottom).

stability of the dimer was evaluated by monitoring the distance between the centre-of-mass (COM) of the monomers, d_{MM} , during 250 ns of cumulative MD (Figure 6).

In DMSO, the starting dimeric species dissociates within 10 ns and remain independently solvated during the rest of the simulation in 3 out of 5 simulations. For this system, one-site rebinding events are also observed but only as transient states. These results are consistent with the dilution experiments in DMSO, which suggest minimal dimerisation of **1a^F** in this polar solvent.

Analogous simulations in a model POPC membrane, starting with a **1a^F** dimer positioned at the centre of the membrane led to the formation of a stable dimer that moves towards the membrane-water interface. In its initial position, the **1a^F** dimer is held together via HB interactions between the squaramide motifs of each monomer (Figure 6). However, as it moves towards the membrane-water interface, interactions with the phosphate head groups of the POPC lipid replace some of the intermolecular HB interactions leading to a one-site binding state ($d_{MM} = 10$ Å). We hypothesise that this dimerisation could compete with anion binding and suppress transport activity.

Conclusions

We have explored the chloride binding and transmembrane transport properties of a family of squaramide-functionalised red-shifted tetra-*ortho*-halo-azobenzenes. These systems act as photo-regulated transmembrane chloride transporters in response to green or red visible light. Comparison of the anion binding properties in solution, molecular dynamics simulations and anion transport experiments in vesicles reveals enhanced

anion binding in the Z isomer compared to the E isomer due to cooperative hydrogen bonds between both squaramide motifs.

By modifying the position of the squaramide substituents, the length of the linker and the nature of tetra-*ortho*-halogen atoms on the azobenzene, we identified that *para*-methylene spacers with tetra-*ortho*-fluoro substituents provide excellent overall activity whilst maintaining a high degree of differentiation of the activities between the E (OFF) and Z (ON) isomers, facilitating efficient photo-switchable anion transport. The transport data and MD simulations point to the role of transporter dimerization in the membrane serving to further diminish the transport activity of the E isomer, which leads to improved OFF-ON switching behaviour of the photo-regulated transport process.

These results demonstrate how control over anion binding affinity, intermolecular interactions between membrane-bound receptors, and subtle changes in transporter geometry in both photo-isomers must all be considered in order to develop photo-switchable ion transporters. We anticipate that these results will provide further design criteria and insights into developing switchable transporters with enhanced differentiation between OFF and ON states, with potential longer term impact in targeted therapeutics.

Conflicts of interest

There are no conflicts to declare

Acknowledgements

A. K. and Z.B. acknowledge the EPSRC Centre for Doctoral Training in Synthesis for Biology and Medicine for a studentship

(EP/L015838/1), generously supported by AstraZeneca, Diamond Light Source, Defence Science and Technology Laboratory, Evotec, GlaxoSmithKline, Janssen, Novartis, Pfizer, Syngenta, Takeda, UCB and Vertex. Z.B. thanks Dr T.K. Piskorz for helpful discussions on MD simulations. MJL acknowledges funding from the Royal Society, the John Fell Oxford University Press Research Fund, and SCG Chemicals Co. Ltd. through the SCG-Oxford Centre of Excellence in Chemistry: SCG Innovation Fund. M. J. L. is a Royal Society University Research Fellow.

Notes and references

‡ The reference binding constants for this analysis were obtained from titration with the simple mono-squaramide receptors **37** and **38**.

- 1 M. Baroncini, S. Silvi and A. Credi, *Chem. Rev.*, 2020, **120**, 200–268.
- 2 V. Blanco, D. A. Leigh and V. Marcos, *Chem. Soc. Rev.*, 2015, **44**, 5341–5370.
- 3 S. P. Jeong, L. A. Renna, C. J. Boyle, H. S. Kwak, E. Harder, W. Damm and D. Venkataraman, *Sci. Rep.*, 2017, **7**, 17773.
- 4 T. J. Kucharski, N. Ferralis, A. M. Kolpak, J. O. Zheng, D. G. Nocera and J. C. Grossman, *Nat. Chem.*, 2014, **6**, 441–447.
- 5 K. Hüll, J. Morstein and D. Trauner, *Chem. Rev.*, 2018, **118**, 10710–10747.
- 6 M. J. Fuchter, *J. Med. Chem.*, 2020, **63**, 11436–11447.
- 7 A. A. Beharry and G. A. Woolley, *Chem. Soc. Rev.*, 2011, **40**, 4422–4437.
- 8 T. Fehrentz, M. Schönberger and D. Trauner, *Angew. Chem. Int. Ed.*, 2011, **50**, 12156–12182.
- 9 D. Bléger, J. Schwarz, A. M. Brouwer and S. Hecht, *J. Am. Chem. Soc.*, 2012, **134**, 20597–20600.
- 10 A. A. Beharry, O. Sadovski and G. A. Woolley, *J. Am. Chem. Soc.*, 2011, **133**, 19684–19687.
- 11 M. Dong, A. Babalhavaeji, C. V. Collins, K. Jarrah, O. Sadovski, Q. Dai and G. A. Woolley, *J. Am. Chem. Soc.*, 2017, **139**, 13483–13486.
- 12 D. B. Konrad, G. Savasci, L. Allmendinger, D. Trauner, C. Ochsenfeld and A. M. Ali, *J. Am. Chem. Soc.*, 2020, **142**, 6538–6547.
- 13 S. Samanta, A. A. Beharry, O. Sadovski, T. M. McCormick, A. Babalhavaeji, V. Tropepe and G. A. Woolley, *J. Am. Chem. Soc.*, 2013, **135**, 9777–9784.
- 14 C. Knie, M. Utecht, F. Zhao, H. Kulla, S. Kovalenko, A. M. Brouwer, P. Saalfrank, S. Hecht and D. Bléger, *Chem. Eur. J.*, 2014, **20**, 16492–16501.
- 15 D. B. Konrad, J. A. Frank and D. Trauner, *Chem. Eur. J.*, 2016, **22**, 4364–4368.
- 16 M. J. Hansen, M. M. Lerch, W. Szymanski and B. L. Feringa, *Angew. Chem. Int. Ed.*, 2016, **55**, 13514–13518.
- 17 R. T. Gephart, D. L. Huang, M. J. B. Aguila, G. Schmidt, A. Shahu and T. H. Warren, *Angew. Chem. Int. Ed.*, 2012, **51**, 6488–6492.
- 18 L. N. Lameijer, S. Budzak, N. A. Simeth, M. J. Hansen, B. L. Feringa, D. Jacquemin and W. Szymanski, *Angew. Chem. Int. Ed.*, 2020, **59**, 21663–21670.
- 19 A. Rullo, A. Reiner, A. Reiter, D. Trauner, E. Y. Isacoff and G. A. Woolley, *Chem. Commun.*, 2014, **50**, 14613–14615.
- 20 M. L. Hammill, G. Islam and J.-P. Desaulniers, *ChemBioChem*, 2020, **21**, 2367–2372.
- 21 V. Poonthiyil, F. Reise, G. Despras and T. K. Lindhorst, *Eur. J. Org. Chem.*, 2018, **2018**, 6241–6248.
- 22 A. Vargas Jentzsch, A. Hennig, J. Mareda and S. Matile, *Acc. Chem. Res.*, 2013, **46**, 2791–2800.
- 23 P. A. Gale, J. T. Davis and R. Quesada, *Chem. Soc. Rev.*, 2017, **46**, 2497–2519.
- 24 J. T. Davis, P. A. Gale and R. Quesada, *Chem. Soc. Rev.*, 2020, **49**, 6056–6086.
- 25 X. Wu, A. M. Gilchrist, P. A. Gale, *Chem*, 2020, **6**, 1296–1309.
- 26 L. E. Bickerton, T. G. Johnson, A. Kerckhoffs and M. J. Langton, *Chem. Sci.*, 2021, DOI: 10.1039/D1SC03545B
- 27 A. V. Jentzsch and S. Matile, in *Halogen Bonding in Solution*, John Wiley & Sons, Ltd, 2021, pp. 195–231.
- 28 L. E. Bickerton, A. J. Sterling, P. D. Beer, F. Duarte and M. J. Langton, *Chem. Sci.*, 2020, **11**, 4722–4729.
- 29 L. E. Bickerton, A. Docker, A. J. Sterling, H. Kuhn, F. Duarte, P. D. Beer and M. Langton, *Chem. Eur. J.*, 2021, DOI:10.1002/chem.202101681.
- 30 M. J. Langton, *Nat. Rev. Chem.*, 2021, **5**, 46–61.
- 31 N. Busschaert, R. B. P. Elmes, D. D. Czech, X. Wu, I. L. Kirby, E. M. Peck, K. D. Hendzel, S. K. Shaw, B. Chan, B. D. Smith, K. A. Jolliffe and P. A. Gale, *Chem. Sci.*, 2014, **5**, 3617.
- 32 X. Wu, J. R. Small, A. Cataldo, A. M. Withecombe, P. Turner and P. A. Gale, *Angew. Chem. Int. Ed.*, 2019, **58**, 15142–15147.
- 33 Y. R. Choi, B. Lee, J. Park, W. Namkung and K.-S. Jeong, *J. Am. Chem. Soc.*, 2016, **138**, 15319–15322.
- 34 M. Fares, X. Wu, D. Ramesh, W. Lewis, P. A. Keller, E. N. W. Howe, R. Pérez-Tomás and P. A. Gale, *Angew. Chem. Int. Ed.*, 2020, **59**, 17614–17621.
- 35 Y. Rin Choi, G. Chan Kim, H.-G. Jeon, J. Park, W. Namkung and K.-S. Jeong, *Chem. Commun.*, 2014, **50**, 15305–15308.
- 36 M. Ahmad, S. Metya, A. Das and P. Talukdar, *Chem. Eur. J.*, 2020, **26**, 8703–8708.
- 37 S. Lee and A. H. Flood, *J. Phys. Org. Chem.*, 2013, **26**, 79–86.
- 38 S. J. Wezenberg, M. Vlatković, J. C. M. Kistemaker and B. L. Feringa, *J. Am. Chem. Soc.*, 2014, **136**, 16784–16787.
- 39 K. Dąbrowa, P. Niedbała and J. Jurczak, *Chem. Commun.*, 2014, **50**, 15748–15751.
- 40 Z. Kokan and M. J. Chmielewski, *J. Am. Chem. Soc.*, 2018, **140**, 16010–16014.
- 41 S. J. Wezenberg and B. L. Feringa, *Nat Commun*, 2018, **9**, 1984.
- 42 X. Chi, W. Cen, J. A. Queenan, L. Long, V. M. Lynch, N. M. Khashab and J. L. Sessler, *J. Am. Chem. Soc.*, 2019, **141**, 6468–6472.
- 43 D. Villarón, M. A. Siegler and S. J. Wezenberg, *Chem. Sci.*, 2021, **12**, 3188–3193.
- 44 A. Docker, X. Shang, D. Yuan, H. Kuhn, Z. Zhang, J. J. Davis, P. D. Beer and M. J. Langton, *Angew. Chem. Int. Ed.*, 2021, DOI:10.1002/anie.202107748.
- 45 A. Kerckhoffs and M. J. Langton, *Chem. Sci.*, 2020, **11**, 6325–6331.
- 46 R. I. Storer, C. Aciro and L. H. Jones, *Chem. Soc. Rev.*, 2011, **40**, 2330–2346.
- 47 A. Kerckhoffs and M. J. Langton, *Chem. Sci.*, 2020, **11**, 6325–6331.
- 48 A. Antoine John and Q. Lin, *J. Org. Chem.*, 2017, **82**, 9873–9876.
- 49 C. A. Hunter and H. L. Anderson, *Angew. Chem. Int. Ed.*, 2009, **48**, 7488–7499.
- 50 C. Coleman, P. J. van Maaren, M. Hong, J. S. Hub, L. T. Costa and D. van der Spoel, *J. Chem. Theory Comput.*, 2012, **8**, 61–74.

ARTICLE

Journal Name

- 51 J. Wang, R. M. Wolf, J. W. Caldwell, P. A. Kollman and D. A. Case, *J. Comput. Chem.*, 2004, **25**, 1157–1174.
- 52 J. Wang, W. Wang, P. A. Kollman and D. A. Case, *J. Mol. Graph. bMod.*, 2006, **25**, 247–260.
- 53 P. Li, L. F. Song and K. M. Merz, *J. Chem. Theory Comput.*, 2015, **11**, 1645–1657.
- 54 M. J. Abraham, D. van der Spoel, E. Lindahl, B. Hess and Gromacs development team, *Gromacs www.gromacs.org*, 2019.
- 55 I. V. Tetko, J. Gasteiger, R. Todeschini, A. Mauri, D. Livingstone, P. Ertl, V. A. Palyulin, E. V. Radchenko, N. S. Zefirov, A. S. Makarenko, V. Yu. Tanchuk and V. V. Prokopenko, *J. Comput. Aid. Mol. Des.*, 2005, **19**, 453–463.
- 56 V. Saggiomo, S. Otto, I. Marques, V. Félix, T. Torroba and R. Quesada, *Chem. Commun.*, 2012, **48**, 5274–5276.
- 57 E. L. Doyle, C. A. Hunter, H. C. Phillips, S. J. Webb and N. H. Williams, *J. Am. Chem. Soc.*, 2003, **125**, 4593–4599.
- 58 L. W. Judd and A. P. Davis, *Chem. Commun.*, 2010, **46**, 2227.
- 59 L. A. Marchetti, L. K. Kumawat, N. Mao, J. C. Stephens and R. B. P. Elmes, *Chem*, 2019, **5**, 1398–1485.
- 60 J. P. M. Jämbeck and A. P. Lyubartsev, *J. Chem. Theory Comput.*, 2012, **8**, 2938–2948.